Wiese, B., Wagner, F., Norden, B., Schmidt-Hattenberger, C. (2017): Fully Coupled Hydrogeophysical Inversion of Hydraulics, Gas Pressure and Geoelectrics. - *Energy Procedia*, *114*, pp. 3588—3596.

DOI: http://doi.org/10.1016/j.egypro.2017.03.1490

Available online at www.sciencedirect.com

ScienceDirect

Energy Procedia 114 (2017) 3588 – 3596

Energy Procedia

13th International Conference on Greenhouse Gas Control Technologies, GHGT-13, 14-18 November 2016, Lausanne, Switzerland

Fully coupled hydrogeophysical inversion of hydraulics, gas pressure and geoelectrics

Bernd U. Wiese[a1], Florian M. Wagner[a,b], Ben Norden[a], Cornelia Schmidt-Hattenberger[a]

[a] *GFZ German Research Centre for Geosciences, Telegrafenberg, 14473 Potsdam,Germany*
[b] *formerly [a], now at University of Bonn, Steinmann Institute, Department of Geophysics, Meckenheimer Allee 176, 53115 Bonn, Germany*

Abstract

The comprehensive interpretation of different data types becomes increasingly challenging, even more if the integration should be carried out in a quantitative manner. A hydrogeophysical reservoir model is set up that links the single phase hydraulics, multiphase behaviour and geoelectrical properties of a CO_2 storage reservoir. The model is embedded into a fully coupled inversion framework that explicitly honours the physical processes underlying the different types of measurement data. The calibrated model provides a comprehensive representation of all data, with an excellent accuracy for hydraulic and gas pressure data and a satisfactory accuracy of arrival times and geoelectrical data. The permeability is within reasonable bounds but the spatial distribution shows several indications for overfitting. The model reproduces the main migration direction of the plume.

Peer-review under responsibility of the organizing committee of GHGT-13.

Keywords: Inverse Modelling; CO_2 Storage; Multiphysics; Pressure; Geoelectric; PEST; Eclipse

1. Introduction

The migration of CO_2 in a reservoir has multiple implications on hydraulic and geophysical properties in the subsurface. Therefore the monitoring concept of CO_2 injection sites is formed by a combination of different monitoring techniques. Methods applied for reservoir monitoring augment continuously. Each individual dataset provides a certain viewpoint on the subsurface that offers the potential to understand reservoir processes much more

1
* Corresponding author. Tel.: +49-331-288-1823; fax: +49-331-288-1529.
E-mail address: bernd.wiese@gfz-potsdam.de

Peer-review under responsibility of the organizing committee of GHGT-13.
doi:10.1016/j.egypro.2017.03.1490

detailed than in the past. Several publications underline the additional value by combining different techniques for monitoring the spreading of the CO_2 plume [1, 2]. Geoelectrical resistivity tomography provides information on the fluid substitution process with comparably high spatiotemporal resolution. Reservoir simulation and geophysical inversions are commonly carried out separately. To achieve the required conformance between models and reservoir behaviour, recent research aims increasingly at coherent interpretation across the disciplines [2]. In practical engineering the amount of data sensitive model parameters grow, wherefore a comprehensive interpretation becomes increasingly challenging. In this work special emphasis is put on advancing the benefit of reservoir modelling by direct and full integration of geoelectric measurements into an inverse reservoir modelling framework, pushing the state of the art of CO_2 reservoir monitoring forward in two main aspects.

- Integration of hydraulic and geophysical data into one hydrogeophysical reservoir model
- Calibration by means on an inverse framework for quantitative evaluation

2. Method

2.1. Geology

The reservoir model is based on a geological facies model. It represents the Stuttgart formation in the eastern part of the Roscow-Ketzin anticline. The horizontal extent is 5 x 5 km and the formation thickness is 90 m. The model consists of two facies types, a sandstone facies with potentially high hydraulic permeability and good reservoir properties and a mudstone facies with poor reservoir properties. Four sandstone reservoir layers are included. The two main layers 1 and 2 with a model thickness of 6 m are divided by a low permeable anhydrite layer and are located in the upper part of the formation (Figure 1). Towards northern direction, only one layer is present. The current geological interpretation considers that layer 1 and layer 2 merge to layer 12 that continues to the northern part. The sandstones permeability and porosity are calibrated in the model, the mudstone is assigned with a fixed permeability of 10^{-4} mD.

2.2. Hydrogeophysical model

The framework consists of a hydrogeophysical reservoir model and an inversion tool (Figure 2). The Hydrogeophysical reservoir model consists of four numerical models. A hydraulic model, a CO_2 migration model and a geoelectrical model. The input for the field generation is a pilot point grid with 428 locations of discrete permeability. The density is higher close to the wells and at the top of the reservoir and decreasing with a larger distance. Model parameter fields are generated based on a linear radial basis function approach and providing permeabilities for all locations of the sandstone facies. Porosities are generated as a function of the permeability based on a petrophysical relation from [3]. The field generator PLPROC [4] is applied. The total simulated period includes the pumping tests between September 2007 and January 2008 and the CO_2 injection history between June 2008 and March 2009.

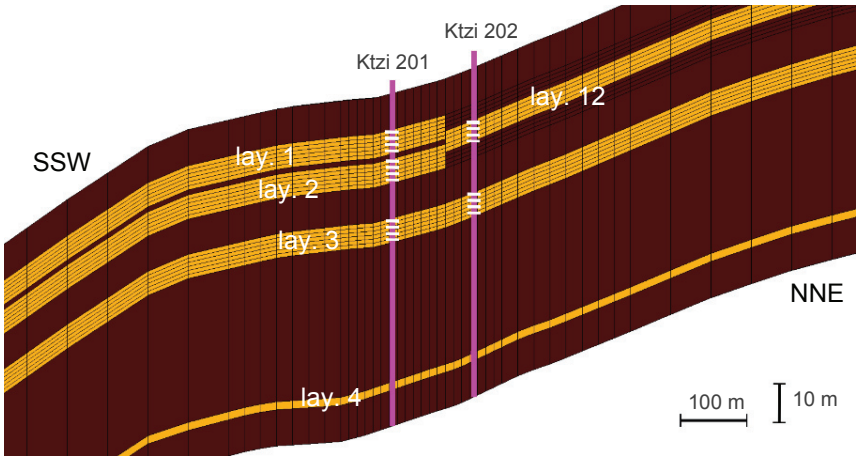

Figure 1: Geological cross section in SSW – NNE direction of the near well area. The orange areas indicate the sandstone facies, brown areas indicate mudstone facies. Wells are magenta, well perforations are indicates by white horizontal lines. Layer 4 is connected to well Ktzi 200 (not shown).

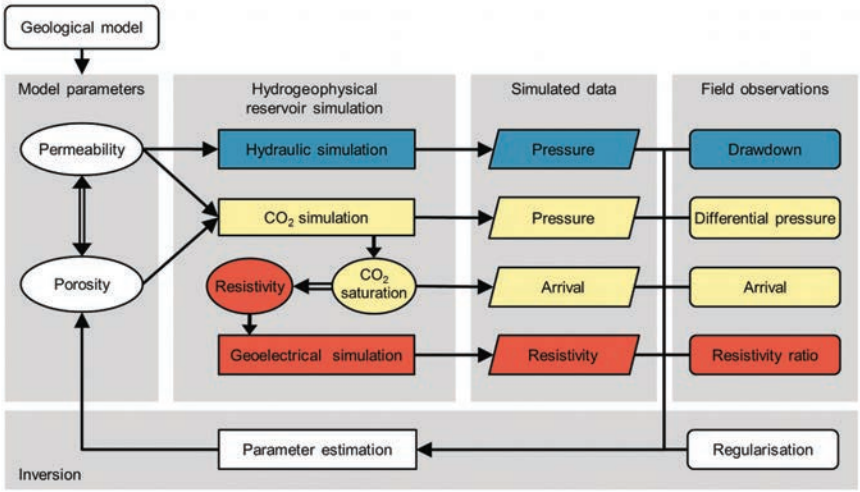

Figure 2: Flowchart of the hydrogeophysical inversion framework. Blue colour indicates the hydraulic branch, yellow colour the CO_2 branch and red colour the geoelectric branch. Ellipses indicate population of the reservoir model, rhombs indicate model generated time series, round cornered boxes indicate constraining data, rectangles represent numerical simulators. Double line arrows indicate petrophysical relations.

2.2.1. Hydraulic simulation

The hydraulic simulation is based on the permeability field only and is carried out with Eclipse 100. Calculated pressure is recalculated with the initial pressure at each test to drawdown values, to avoid impairment from potential reference level errors. The measurement data are acquired during three cross-hole pumping tests have been carried out at Ketzin prior to CO_2 injection. Formation fluid was pumped from one well with pressure observation in the pumping well and two further observation wells. These tests have been evaluated with traditional analytical pumping test evaluation methods [5] and have been modelled with an inverse hydraulic model [6]. Until now, no agreement with the Ketzin reservoir model could be achieved.

2.2.2. CO_2 simulation

The injection rates are shown in Figure 3a and exhibit many short term variations due to technical reasons. These small term variations are averaged over a longer period to reduce the model runtime. For the choice of periods the most important criteria is that the modelled and measured injection rates match exactly at the last hours of each interval, when the reservoir pressure is picked for the calibration dataset. Errors in the raw injection rate are removed by cross checking with pressure and DTS temperature recordings in the injection well.

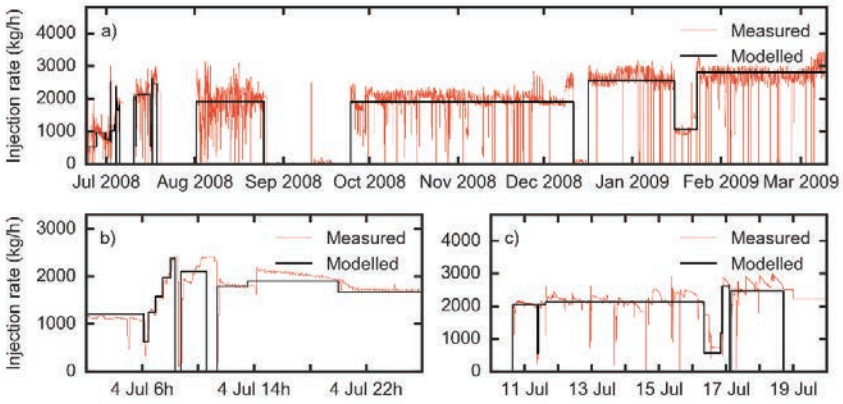

Figure 3: Injection rates in well Ktzi 201. The red curve shows raw data of measured rates with 5 minute intervals, the black curve shows the averaged rates used for the model. Recording errors can be observed in subfigure b) at July, 4th at 10.30 and in subfigure c) at July 19th and are corrected by cross checking with reservoir pressure and DTS temperature recordings.

The CO_2 simulation is based on the permeability and porosity field and is carried out with Eclipse 300. The long term trend is calculated analogue to hydraulics by subtracting the initial pressure from each observed value. Additionally, a short term differential pressure is introduced that is calculated from the pressure before and after each change of injection rate. This ensures that the short term dynamic of the model is captured. Further, the arrival times of the CO_2 in both observation wells are used as calibration data.

The CO_2 bottom hole pressure has been monitored continuously in the injection well during site operation. The arrival of the CO_2 has been recorded in the two observation wells. A previous reservoir model was manually calibrated on the CO_2 specific reservoir data only [7].

2.2.3. Geoelectric simulation

The geoelectric simulation is carried out based on the porosity field and the CO_2 saturation field as calculated by the CO_2 migration model using the open source simulator pyGIMLi [8]. Three Ketzin boreholes are equipped with 15 geoelectric bottomhole electrodes each. A large number of four electrode measurements in single- and cross-hole configurations has been carried out with a weekly interval [9]. In previous approaches the entire geoelectrical data set has been inverted separately and the CO_2 plume shape was derived (e.g. [1, 9]).
In the current approach, the required coverage is lower because the CO_2 migration model acts as external regularisation. Therefore the quality criteria can be stricter. Most electrodes are located within an open annulus that is filled by brine or CO_2 which is known to produce artifacts [10]. Therefore only electrodes that are located within a cemented annulus are selected. The inherent noise level of geoelectrical arrays is reduced by applying a moving median of the individual measurements. From 1008 raw configurations only 8 are used as calibration data.

The base noise level of the measurements is reduced by normalising the observed resistivities of each configuration with the respective baseline resistivity prior to CO_2 injection. The resulting apparent resistivity ratio is a function of partial CO_2 saturation. The interdependence of partial brine saturation and geoelectrical properties is honored by an experimentally determined petrophysical relation [11, 12].

2.3. Inversion

The need for repeated individual inversions is circumvented by directly feeding the entire data into the fully-coupled hydrogeophysical inversion. The PEST inversion package [13] provides the platform to couple different process simulators and the corresponding multiple data sets. Assisted singular value decomposition reduces the dimensionality of the inverse problem resulting in a lower number of model runs compared to traditional inversion approaches.

The model includes four different types of measurement data: Hydraulic data, CO_2 pressure data, CO_2 arrival times and geoelectric data. These data represent different times, measurement intervals, physical units and range of values. The goal is to provide a balanced weighting for all series. The individual data series are weighted such that they have an equal contribution to the measurement objective function for an equal relative deviation from the observed values.

The model has 434 free parameters. Of these are 428 spatially distributed permeability values, other parameters are rock compressibility, relative permeability parameters, equivalent pore volumes representing the model boundaries and the exponent relating the reservoir saturation to a corresponding electrical conductivity. The dimensionality of the current problem could be reduced by factor seven to 60 superparameters. Each super parameter represents a linear combination of the free model parameters.

A preferred value regularisation constraint is added to all parameters. This value represent a best a priory estimation. This ensures numerical stability of the inversion scheme if parameters become numerically insensitive, in all other cases, i.e. when the measurement objective function is affected, the weight is adjusted such that regularisation becomes negligible.

3. Results and discussion

3.1. Hydraulics

The hydraulic drawdowns show a good match between measured and simulated data (Figure 4). The absolute deviations are highest if the pump is located in the respective observation wells. For “o201 p201” for example the deviation is almost 1 bar at the last measurement. In the combination “o200 p202” the same relative deviation is only 0.07 bar. The weighting scheme ensures that relative deviations are similar for all plots. The weighting scheme ensures that the maximum relative deviation is about 10% of the dynamic of the respective time series.

The two well combinations involving Ktzi 200 and Ktzi 201 are removed from the calibration dataset. No solution with a satisfactory curve match of both time series could be found. Inclusion either of both time series results in large areas with permeabilities at their imposed lower and upper boundaries of 1 or 1000 mD, strongly indicating overfitting. An error of both time series appears plausible, since the same pressure logger was used.

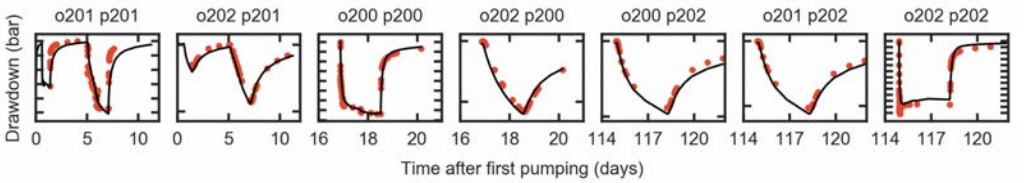

Figure 4: Measured drawdown of the pre-injection pumping tests (red circles) and corresponding simulations (black lines). The ticks at y-axes each represent 1 bar differential pressure. The first part of the title beginning with "o" refers to the observation well, the second part of the title, beginning with "p" refers to the corresponding pumping well.

3.2. CO_2 migration

The simulated CO_2 reservoir pressure shows a good overall match with the measured data (Figure 5a). Generally, the absolute deviations are around 0.3 bar with a maximal value of 1.6 bar in January 2009. After injection start at the end of June, the size of the plume is small and located close to the injection well, wherefore rapid rate variations are explicitly included in the inversion to capture the reservoir behaviour on different spatial and temporal scales. The short term dynamics with a magnitude of 0.2 bar are well reproduced, although an offset of about one bar exists (Figure 5b). This is achieved since short and long term variations are calibrated as separate datasets that orthogonalises out structural noise of an (necessarily always) imperfect model [14]. A direct calibration of pressures would lead to an unphysical trade-off as e.g. a flat inverted pressure curve with less offset. Simulated arrival times are 22.9 and 259 days with observed values of 21 and 270 day in Ktzi 200 and Ktzi 202, respectively.

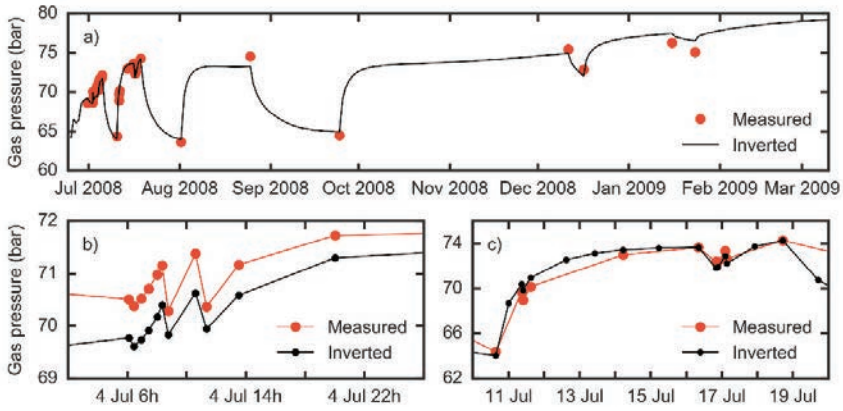

Figure 5: Measured reservoir pressure at the end of the respective time series (red) and the corresponding inverted pressure (black).

3.3. Geoelectric

The objective function of the geoelectric resistivities was reduced by factor 5. Four examples of calibrated curves are shown in Figure 6. A sufficient match of the data is shown in Figure 6a and 6d. The resistivity ratios generally show an increasing trend, honouring the increased reservoir resistivity due to the low conductivity CO_2. However, AB-MN electrode configurations have some areas with negative sensitivity, i.e. an increasing resistivity in the reservoir may induce a decreasing apparent resistivity. This impact can be observed in the first 50 days of Figure 5b and for Figure 5c. The current model cannot reproduce the negative sensitivities, wherefore the goodness of fit is lower compared to the pressure data.

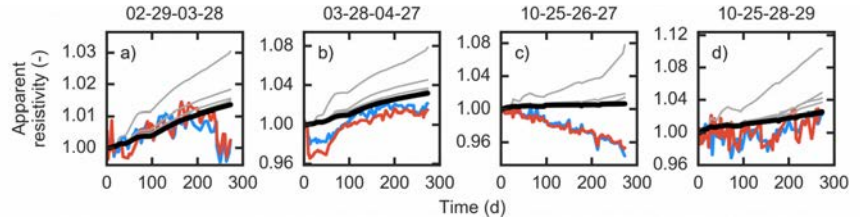

Figure 6: Apparent resistivity ratios of the applied electrode configurations. The red and blue curve indicate the moving median of reciprocal measurements, the grey curves indicate the change of simulated resistivity ratios during 4 iterations, the black curve is the final result of the 5th iteration. The x axis indicates days since the injection of CO_2. The titles refer to the a-b-m-n electrode configuration.

3.4. Parameter distribution

The calibrated permeability shows a spatial variability with values between the imposed parameter bounds 1 and 1000 mD, while the permeability of 10^{-4} is imposed by the geological model (Figure 7). Although the permeability is generally within a realistic range some structural aspects suggest that overfitting occurs. Large areas are identical to the parameter bounds, although core analyses of the observation wells show a variability of less than one order of magnitude for the depth averaged effective permeability. The wells are inflection points for permeability changes. Permeability is low between the lower wells in layer 1 while it is high in the opposite direction (Figure 7a). This distribution coincides with the sensitivity pattern of cross-hole pumping tests. Furthermore, large variations close to the wells occur also in layer 2 and layer 12. From a geostatistical point of view, it is unlikely that the field permeability in the wells is similar to each other while the simulated permeabilities show such a high variability.

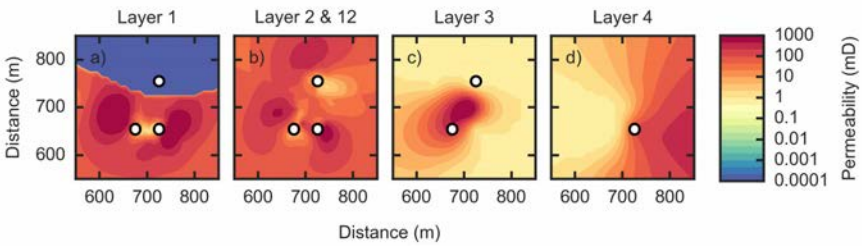

Figure 7: Calibrated reservoir permeability. The dots represent screened well positions, with the western dot is the injection well Ktzi 201. Note that the dot in layer 4 is the observation well Ktzi 200.

The layered structural elements of the permeability are shaping the plume. The plume shape has a predominantly westward direction, analogue to the observed migration direction [2]. The shape differs between the layers. Most CO_2 is located in layer 1 and 2, which are considered as the main reservoir layers. The plume in layer 3 is limited to the direct vicinity of the well. The plume in layer 4 (Figure 8d) appears around observation well Ktzi 200 since the overpressure is sufficient to exceed the static hydraulic pressure of the brine column between layer 2 and layer 4.

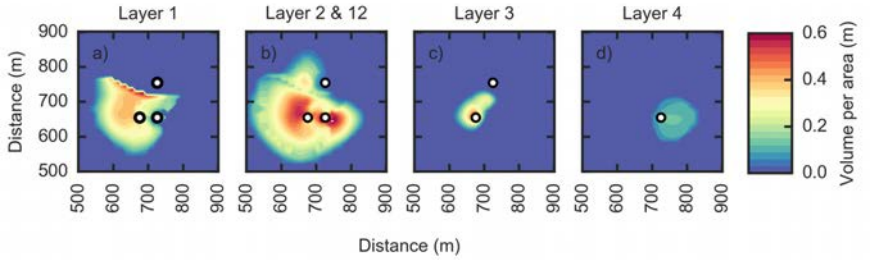

Figure 8: Calibrated CO_2 thickness at the end of the simulation period after 270 days. It represents the porosity occupied by CO_2 in m³ per area in m². The dots represent screened well positions, with the western dot is the injection well Ktzi 201. Note that the dot in layer 4 is the observation well Ktzi 200.

4. Conclusions

A hydrogeophysical reservoir model is set up that links the single phase hydraulics, multiphase behaviour and geoelectrical properties of a CO_2 storage system. The model is embedded into an inversion framework. The calibrated model provides a satisfying representation of all data, with an excellent accuracy for hydraulic and CO_2 pressure and a satisfactory representation of arrival times and geoelectrical data. The model can reproduce the main migration direction of the plume. The estimated permeability is within reasonable bounds but the spatial distribution of the current model shows indications of overfitting. Investigation of this overfitting is subject of current research.

References

[1] Bergmann, P., Ivandic, M., Norden, B., Rücker, C., Kiessling, D., Lueth, S., Schmidt-Hattenberger, C., Juhlin, C. (2014): Combination of seismic reflection and constrained resistivity inversion with an application to 4D imaging of the CO2 storage site, Ketzin, Germany. - Geophysics, 79, 2, p. B37-B50.

[2] Lüth, S.; Ivanova, A. & Kempka, T. (2015), 'Conformity assessment of monitoring and simulation of CO<inf>2</inf> storage: A case study from the Ketzin pilot site', International Journal of Greenhouse Gas Control 42, 329-339.

[3] Norden, B. & Frykman, P. (2013), 'Geological modelling of the Triassic Stuttgart Formation at the Ketzin CO2 storage site, Germany', International Journal of Greenhouse Gas Control 19, 756-774.

[4] Doherty, J. (2015), 'PLPROC - A Parameter List Processor', Technical report, National Centre for Groundwater Research and Training, Australia and Watermark Numerical Computing.

[5] Wiese, B.; Böhner, J.; Enachescu, C.; Würdemann, H. & Zimmermann, G. (2010), 'Hydraulic characterisation of the Stuttgart formation at the pilot test site for CO2 storage, Ketzin, Germany', International Journal of Greenhouse Gas Control 4, 960-971.[6] Chen, F.; Wiese, B.; Zhou, Q.; Kowalsky, M.; Norden, B.; Kempka, T. & Birkholzer, J. (2014), 'Numerical modeling of the pumping tests at the Ketzin pilot site for CO2 injection: Model calibration and heterogeneity effects', International Journal of Greenhouse Gas Control 22, 200-212.

[7] Kempka, T. & Kühn, M. (2013), 'Numerical simulations of CO2 arrival times and reservoir pressure coincide with observations from the Ketzin pilot site, Germany', Environmental Earth Sciences 70(8), 3675-3685.

[8] Rücker, C.; Günther, T. & Wagner, F. M. (2015), 'Coupled hydrogeophysical modelling and ERT monitoring using pyGIMLi"3rd International Workshop on Geoelectrical Monitoring - GELMON (Vienna 2015), http://www.pygimli.orghttp://www.pygimli.org'.

[9] Schmidt-Hattenberger, C.; Bergmann, P.; Labitzke, T.; Wagner, F. & Rippe, D. (2016), 'Permanent crosshole electrical resistivity tomography (ERT) as an established method for the long-term CO2 monitoring at the Ketzin pilot site', International Journal of Greenhouse Gas Control 52, 432-448.

[10] Wagner, F.M..; Bergmann, P.; Rücker, C.; Wiese, B.; Labitzke, T.; Schmidt-Hattenberger, C. & Maurer, H. (2015), 'Impact and mitigation of borehole related effects in permanent crosshole resistivity imaging: An example from the Ketzin CO2 storage site', Journal of Applied Geophysics 123, 102-111.

[11] Kummerow, J. & Spangenberg, E. (2011), 'Experimental evaluation of the impact of the interactions of CO2-SO$_2$, brine, and reservoir rock on petrophysical properties: A case study from the Ketzin test site, Germany', Geochemistry, Geophysics, Geosystems 12, Q05010.

[12] Wagner, Florian Michael. New developments in electrical resistivity imaging with applications to geological CO_2 storage. ETH-Zürich (2016). http://dx.doi.org/10.3929/ethz-a-010636965.

[13] Doherty, J. (2016), 'PEST - Model-Independent Parameter Estimation User Manual Part 1: PEST, SENSAN and Global Optimisers'(6th Edition), Technical report, Watermark Numerical Computing.

[14] Wiese, B. & Nützmann, G. (2011), 'Calibration of spatial aquitard distribution using hydraulic head changes and regularisation', Journal of Hydrology 408(1-2), 54-66.